Inorg. Chem. **2006**, *45*, 4261–4267

Macrocyclic Amines as Structure-Directing Agents for the Synthesis of Three-Dimensional Antimony-Sulfide Frameworks

Anthony V. Powell,*,† Rachel J. E. Lees,† and Ann M. Chippindale‡

Department of Chemistry, Heriot-Watt University, Edinburgh EH14 4AS, U.K., and School of Chemistry, The University of Reading, Whiteknights, Reading RG6 6AD, U.K.

Received February 15, 2006

A new family of antimony sulfides, incorporating the macrocyclic tetramine 1,4,8,11-tetraazacyclotetradecane (cyclam), has been prepared by a hydrothermal method. $[C_{10}N_4H_{26}][Sb_4S_7]$ **(1)**, $[Ni(C_{10}N_4H_{24})][Sb_4S_7]$ **(2)**, and $[Co(C_{10}N_4H_{24})]_x[C_{10}N_4H_{26}]_{1-x}[Sb_4S_7]$ $(0.08 \leq x \leq 0.74)$ **(3)** have been characterized by single-crystal X-ray diffraction, elemental analysis, thermogravimetry, and analytical electron microscopy. All three materials possess the same novel three-dimensional $Sb_4S_7^{2-}$ framework, constructed from layers of parallel arrays of $Sb_4S_8^{4-}$ chains stacked at 90° to one another. In **1**, doubly protonated macrocyclic cations reside in the channel structure of the antimony-sulfide framework. In **2** and **3**, the cyclam acts as a ligand, chelating the divalent transition-metal cation. Analytical and X-ray diffraction data indicate that the level of metal incorporation in **2** is effectively complete, whereas in **3**, both metalated and nonmetalated forms of the macrocycle coexist within the structure.

Introduction

Template-directed synthesis of chalcogenides is of increasing interest in the search for new materials with novel architectures.[1] The report by Bedard and co-workers[2] that solvothermal methods adapted from those used in oxide and, particularly, zeolite chemistry could be used to effect the synthesis of tin and germanium sulfides led to a tremendous growth in template-directed synthesis of main-group chalcogenides. Much attention has subsequently focused on the sulfides of germanium, indium, and antimony, which exhibit a range of interesting structural features, including low-dimensionality,[3,4,5,6,7,8] adamantoid building units,[9,10] supertetrahedra,[11,12] and zeolitic-like structures.[13]

Synthesis of these materials is generally performed in the presence of organic amines as structure-directing agents. The principal types of organic species used are linear and branched long-chain aliphatic amines and polyamines and alicyclic amines. Long-chain polyamines, in particular, are frequently unstable at elevated temperatures.[14] For example, under solvothermal conditions they can undergo side-reactions such as cyclization[3,15] and cleavage,[16] thereby introducing further geometric diversity into the structure-directing agent. The products of such reactions consist of complex anionic metal-sulfide frameworks with protonated amines fulfilling the charge-balancing role.

The introduction of transition-metal cations into the reaction mixture usually leads to chelation and the in situ formation of a transition-metal-amino complex. Such complexes can themselves serve as structure-directing agents for the growth of anionic main-group sulfide frameworks. For example, tris(ethylenediamine) complexes of iron, cobalt, and nickel serve as charge-balancing counterions for anionic

* To whom correspondence should be addressed. Fax: +44 (0)131 451 3180. E-mail: a.v.powell@hw.ac.uk.
† Heriot-Watt University.
‡ The University of Reading.

(1) Feng, P.; Bu, X.; Zheng, N. *Acc. Chem. Res.* **2005**, *38*, 293.
(2) Bedard, R. L.; Wilson, S. T.; Vail, L. D.; Bennett, J. M.; Flanigen, E. M. In *Zeolites: Facts, Figures, Future;* Jacobs, P., van Santen, R. A., Eds.; Elsevier: Amsterdam, 1989.
(3) Parise, J. B.; Ko, Y. *Chem. Mater.* **1992**, *4*, 1446.
(4) Bensch, W.; Schur, M. *Z. Naturforschung.* **1997**, *52b*, 405.
(5) Stephan, H.-O.; Kanatzidis, M. G. *Inorg. Chem.* **1997**, *36*, 6050.
(6) Tan, K.; Ko, Y.; Parise, J. *Acta Crystallogr.* **1994**, *C50*, 1439.
(7) Wang, X. *Eur. J. Solid State Inorg. Chem.* **1995**, *32*, 303.
(8) Tan, K.; Ko, Y.; Parise, J. B.; Park, J. B.; Darovsky, A. *Chem. Mater.* **1996**, *8*, 206.
(9) Cahill, C. L.; Parise, J. B. *Chem. Mater.* **1997**, *9*, 807.
(10) MacLachlan, M.; Coombs, N.; Ozin, G. A. *Nature* **1999**, *397*, 681.
(11) Cahill, C. L.; Younghee, K.; Parise, J. B. *Chem. Mater.* **1998**, *10*, 19.
(12) Li, H.; Kim, J.; O'Keeffe, M.; Yaghi, O. M. *Angew. Chem., Int. Ed.* **2003**, *42*, 1819.
(13) Vaqueiro, P.; Chippindale, A. M.; Powell, A. V. *Inorg Chem.* **2004**, *43*, 7963.
(14) Hutchinson, W. M.; Collett, A. R.; Lazzell, C. L. *J. Am. Chem. Soc.* **1945**, *67*, 1966.
(15) Powell, A. V.; Paniagua, R.; Vaqueiro, P.; Chippindale, A. M. *Chem. Mater.* **2002**, *14*, 1220.
(16) Lees, R. J. E.; Powell, A. V.; Chippindale, A. M. *Acta Crystallogr.* **2005**, *C61*, m516.

10.1021/ic060263f CCC: $33.50
Published on Web 04/22/2006

SbS_2^- and $Sb_4S_7^{2-}$ infinite chains in $[M(en)_3][Sb_2S_4]$ and $[M(en)_3][Sb_4S_7]$,[5] respectively, while $Co(en)_3^{2+}$ ions reside in one-dimensional channels and balance the charge of the anionic $Sb_{12}S_{19}^{2-}$ framework in $[Co(en)_3][Sb_{12}S_{19}]$.[13] Bis(diethylenetriamine) complexes of iron and nickel fulfill a similar role for the layered anions in $[Fe(C_4H_{13}N_3)_2]Sb_6S_{10}\cdot 0.5H_2O$,[17] $[Ni(C_4H_{13}N_3)_2]Sb_{22}S_{42}\cdot 0.5H_2O$,[18] and $[Ni(C_4H_{13}N_3)_2]Sb_4S_7\cdot H_2O$.[19] In $[Ni(C_4H_{13}N_3)_2]_2[Sb_4S_8]$[20] and $[Ni(C_4H_{13}N_3)_2]_3[Sb_3S_6]_2$,[21] the $Sb_xS_y^{z-}$ anions and charge-balancing $Ni(C_4H_{13}N_3)_2^{2+}$ cations are isolated and held together by relatively weak secondary interactions, giving the materials saltlike characteristics. Clearly in all such cases, the presence of the transition-metal cation is an essential prerequisite for the templating agent to exist, and formation of the corresponding nonmetalated phase is impossible.

In this work, a macrocyclic tetramine has, for the first time, been used as a structure-directing agent. Remarkably, we have succeeded in preparing new three-dimensional antimony sulfides containing 1,4,8,11-tetraazacyclotetradecane (cyclam) both as the protonated uncoordinated macrocycle in $[C_{10}N_4H_{26}][Sb_4S_7]$ **(1)** and as a chelating complex with transition-metal cations in $[Ni(C_{10}N_4H_{24})][Sb_4S_7]$ **(2)**. Moreover, the third phase reported, $[Co(C_{10}N_4H_{24})]_x[C_{10}N_4H_{26}]_{1-x}[Sb_4S_7]$ **(3)**, contains both metalated and nonmetalated forms. This work suggests that macrocycles, which do not show any selectivity toward the complexation of transition-metal ions in aqueous solution, may, when used as structure-directing agents in framework-sulfide synthesis, provide a means of combining the selectivity inherent in porous structures with the narrow and tunable band gap of chalcogenides, leading to multifunctional materials.[1]

Experimental Section

Single crystals of $[C_{10}N_4H_{26}][Sb_4S_7]$ **(1)**, $[Ni(C_{10}N_4H_{24})][Sb_4S_7]$ **(2)**, and $[Co(C_{10}N_4H_{24})]_x[C_{10}N_4H_{26}]_{1-x}[Sb_4S_7]$ **(3)** were prepared under hydrothermal conditions. For **1**, cyclam (0.300 g, 1.5 mmol), Sb_2S_3 (0.679 g, 2 mmol), and S (0.160 g, 5 mmol) were stirred with 3 mL of deionized water in a 23 mL Teflon-lined stainless steel autoclave to give a mixture with an approximate molar composition ratio for Sb:S:cyclam of 4:11:1.5. The mixture was heated at 438 K for 4 days and cooled to room temperature at 20 K h^{-1}. The solid product was filtered, washed in deionized water and acetone, and dried in air at room temperature. The product contained yellow blocks of **1** as the major phase, a number of red blocks, and a few orange blocks, together with a small amount of black powder, that was identified by powder X-ray diffraction as unreacted Sb_2S_3. Single-crystal X-ray diffraction identified the orange blocks as the new phase $[C_{10}N_4H_{26}][Sb_6S_{10}]$[22] and the red blocks as the previously reported $[C_2H_{10}N_2][Sb_8S_{13}]$.[6] Combustion analysis of a hand-picked sample of **1** found C = 13.03, H = 2.58, and N = 6.10%, in excellent agreement with values of C = 13.14, H = 2.87, and N = 6.13%, calculated for the formula $[C_{10}N_4H_{26}][Sb_4S_7]$.

Crystals of **2** and **3** were prepared under analogous conditions and reagent concentrations. Transition-metal salts (for **2**, $NiSO_4\cdot 7H_2O$ (0.505 g, 1.8 mmol), and for **3**, $Co(O_2CCH_3)_2$ (0.409 g, 1.65 mmol)) were mixed with the cyclam and deionized water, prior to the addition of Sb_2S_3 and S. After the mixture had reacted for 4 days at 438 K and cooled at 20 K h^{-1}, the solid product was isolated as above. The product of the reaction containing $NiSO_4\cdot 7H_2O$ consisted of dark-yellow blocks of **2** as the major phase, together with a small amount of black powder, identified by powder X-ray diffraction as unreacted Sb_2S_3. Combustion analysis for the crystals of (**2**) gave C = 12.12, H = 2.32, and N = 5.62% (calcd for formula $[Ni(C_{10}N_4H_{24})][Sb_4S_7]$: C = 12.38, H = 2.49, and N = 5.77%). The product from the reaction to which $Co(O_2CH_3)_2$ was added consisted of yellow blocks of **3** as the majority phase, together with red blocks of $[C_2H_{10}N_2][Sb_8S_{13}]$[6] and a small amount of black powder. The last was identified as a mixture of CoS_2 and unreacted Sb_2S_3 by powder X-ray diffraction of the bulk product. Combustion analysis of **3** was not performed because of the variation in Co content between crystals that was established by analytical electron microscopy (vide infra).

The hand-picked single crystals of **1**, **2**, and **3** were further characterized by analytical electron microscopy and, for **1** and **2**, thermogravimetric analysis. Analytical electron microscopy was carried out using a Philips XL30 scanning microscope equipped with an EDAX "Phoenix" detection system. The Sb:S ratios of 0.59(3), 0.61(2), and 0.59(3) obtained for **1**, **2**, and **3**, respectively, are in good agreement with the value of 0.57 for the crystallographic formulas determined below. For **2**, all crystallites examined contained Ni with an average Ni:S ratio of 0.14(1), corresponding to a nickel site occupancy of 0.98(7). This is consistent, within experimental error, with each cyclam macrocyclic ring containing a nickel cation. However, for **3**, a considerably larger variation in the Co:S ratio was observed (ca. 0.01−0.1), indicative of partial occupancy by cobalt of the site at the center of the macrocyclic ring, over the range of 0.08−0.74. Although a number of additional syntheses were carried out with varying reactant stoichiometries, similar variations in cobalt content were observed in the products of all reactions, which produced single crystals of **3**. Thermogravimetric analysis was carried out using a Dupont Instruments 951 Thermal Analyzer. Approximately 4−5 mg of finely ground crystals of **1** and **2** were heated under a flow of dry nitrogen over the temperature range of 298−673 K at a heating rate of 15 K min^{-1}. A single weight loss of 22.00% was observed for **1** (onset 558 K), which compares very well with the value of 22.14% calculated for the complete loss of the organic component. For **2**, a single weight loss of 18.67% occurs at T = 606 K. The discrepancy between this and the value of 20.64% expected for loss of the organic component is accounted for by the observation that the product of thermogravimetric analysis contained residual organic material (2.98%), giving a total organic content of 20.65%. The powder X-ray diffraction patterns of the thermal decomposition products indicate that they are amorphous.

Crystal Structure Determination. X-ray intensity data for $[C_{10}N_4H_{26}][Sb_4S_7]$ **(1)**, $[Ni(C_{10}N_4H_{24})][Sb_4S_7]$ **(2)**, and $[Co(C_{10}N_4H_{24})]_x[C_{10}N_4H_{26}]_{1-x}[Sb_4S_7]$ ($x \approx 1/3$) **(3)** were collected at 100 K, after rapid cooling from room temperature, using a Bruker-AXS X8 Apex CCD diffractometer with graphite-monochromated Mo Kα radiation (λ = 0.71073Å). Data were processed using the manufacturer's standard routines.[23] Full crystallographic details are given in Table 1.

(17) Stähler, R.; Näther, C.; Bensch, W. *Eur. J. Inorg. Chem.* **2001**, 1835.
(18) Stähler, R.; Bensch, W. *Z. Anorg. Allg. Chem.* **2002**, *628*, 1657.
(19) Stähler, R.; Näther, C.; Bensch, W. *J. Solid State Chem.* **2003**, *174*, 264.
(20) Bensch, W.; Näther, C.; Stähler, R. *Chem Commun*. **2001**, 477.
(21) Kiebach, R.; Studt, F.; Näther, C.; Bensch, W. *Eur. J. Inorg. Chem.* **2004**, 2553.
(22) Lattice parameters for $[C_{10}N_4H_{26}][Sb_6S_{10}]$ at 100 K: *P2₁/c*, a = 9.4872(9) Å, b = 15.447(1) Å, c = 10.7567(9) Å, and β = 105.878(4)°.
(23) *APEX-2*, version 1.27; Bruker AXS Inc.: Madison, WI, 2005.
(24) Altomare, A.; Cascarano, G.; Giacovazzo, G.; Guagliardi, A.; Burla, M. C.; Polidori, G.; Camalli, M. *J. Appl. Crystallogr*. **1994**, *27*, 435.

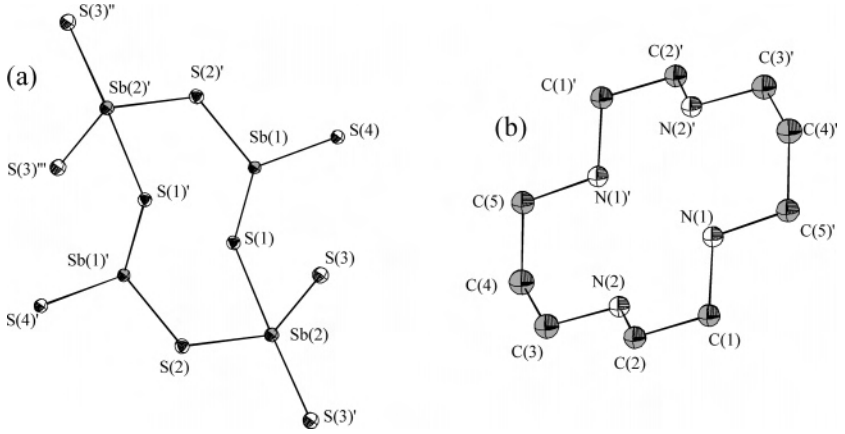

Figure 1. Local coordination of (a) nontemplate atoms and (b) the carbon−nitrogen ring of the template in $[C_{10}N_4H_{26}][Sb_4S_7]$ **(1)**, showing the atom labeling scheme and ellipsoids at 50% probability.

Table 1. Crystallographic Data for $[C_{10}N_4H_{26}][Sb_4S_7]$ (**1**), $[Ni(C_{10}N_4H_{24})][Sb_4S_7]$ (**2**), and $[Co(C_{10}N_4H_{24})]_x[C_{10}N_4H_{26}]_{1-x}[Sb_4S_7]$ (**3**)

	1	**2**	**3**
formula	$[C_{10}H_{26}N_4][Sb_4S_7]$	$[Ni(C_{10}N_4H_{24})][Sb_4S_7]$	$[Co(C_{10}N_4H_{24})]_x[C_{10}N_4H_{26}]_{1-x}$ $[Sb_4S_7]$ ($x \approx 1/3$)
M_r	913.88	970.55	933.51
crystal system	monoclinic	monoclinic	monoclinic
crystal habit	yellow block	dark yellow block	dark yellow block
crystal dimensions (mm)	0.12 × 0.12 × 0.05	0.16 × 0.16 × 0.08	0.20 × 0.16 × 0.04
space group	*C*2/*c*	*C*2/*c*	*C*2/*c*
T (K)	100	100	100
a (Å)	13.7125 (5)	13.7781 (5)	13.6001(7)
b (Å)	11.8863 (4)	11.8694 (5)	11.9193(6)
c (Å)	15.4368 (6)	15.3855 (7)	15.4311(8)
β (deg)	102.712 (2)	102.772 (2)	102.557(3)
V (Å^3)	2454.39 (16)	2453.86 (18)	2441.6(2)
Z	4	4	4
μ (mm^{-1})	4.957	5.702	5.205
ρ_{calc} (Mg m^{-3})	2.473	2.627	2.540
measured data	32 291	25 506	40 082
unique data	3729	3733	3704
obsd data ($I \geq 3\sigma(I)$)	2658	1879	2033
R_{int}	0.031	0.052	0.047
residual electron density (min, max) (e Å^{-3})	−0.64, 1.20	−1.19, 0.95	−0.89, 0.79
params refined	114	120	121
$R(F)$	0.0193	0.0289	0.0232
$R_w(F)$	0.0199	0.0324	0.0257

The structures were solved using the direct methods program SIR92,[24] and all non-hydrogen atoms were located. The CRYSTALS suite of programs[25] was used for subsequent refinements against *F*. All the hydrogen atoms in **1** could be located in difference Fourier maps but were placed geometrically during refinement. Geometric placement was used from the start for the hydrogen atoms in **2** and **3**.

In the final cycles of refinement, anisotropic thermal parameters were refined for all non-hydrogen atoms. In **2** and **3**, site-occupancy factors of the transition metal were treated as refinable parameters yielding final refined values of 0.953(6) and 0.339(5), respectively, which are in good agreement with the conclusions reached from the analytical electron microscopy.

Results and Discussion

Figure 1 shows the local coordination of the framework atoms of **1**, and selected bond lengths and angles are presented in Table 2. One of the two crystallographically distinct antimony atoms in the asymmetric unit, Sb(1), exhibits trigonal pyramidal coordination by sulfur with

Table 2. Selected Bond Lengths (Å), Angles (deg), and Bond Valences (v.u.) for $[C_{10}N_4H_{26}][Sb_4S_7]$ (**1**)[b]

		ν[a]		
Sb(1)−S(2)^i	2.4883 (7)	0.893	S(2)^i−Sb(1)−S(1)^i	83.61 (2)
Sb(1)−S(1)^i	3.0697 (7)	0.162	S(2)^i−Sb(1)−S(1)	96.70 (2)
Sb(1)−S(1)	2.4100 (7)	1.125	S(1)^i−Sb(1)−S(1)	84.25 (2)
Sb(1)−S(4)	2.5390 (6)	0.770	S(2)^i−Sb(1)−S(4)	89.74 (2)
	Σ	**2.950**	S(1)^i−Sb(1)−S(4)	172.31(2)
Sb(2)−S(3)^{ii}	2.7119 (8)	0.463	S(1)−Sb(1)−S(4)	92.72 (2)
Sb(2)−S(1)	2.7520 (7)	0.411	S(3)^{ii}−Sb(2)−S(1)	175.80 (2)
Sb(2)−S(2)	2.4556 (7)	0.984	S(3)^{ii}−Sb(2)−S(2)	88.19 (2)
Sb(2)−S(3)	2.3839 (7)	1.215	S(1)−Sb(2)−S(2)	91.32 (2)
	Σ	**3.073**	S(3)^{ii}−Sb(2)−S(3)	86.94 (2)
			S(1)−Sb(2)−S(3)	89.09 (2)
			S(2)−Sb(2)−S(3)	102.30 (3)

[a] Bond valences and their sums calculated using parameters from ref 30. [b] Symmetry codes: (i) 2 − *x*, −*y*, 1 − *z*; (ii) 5/2 − *x*, 1/2 − *y*, 1 − *z*; (iii) 3/2 − *x*, 1/2 − *y*, 1 − *z*; (iv) 2 − *x*, *y*, 3/2 − *z*.

(25) Watkin, D. J.; Prout, C. K.; Carruthers, J. R.; Betteridge, P. W.; Cooper, R. I. *CRYSTALS*, issue 11; Chemical Crystallography Laboratory, University of Oxford: Oxford, U.K., 2001.

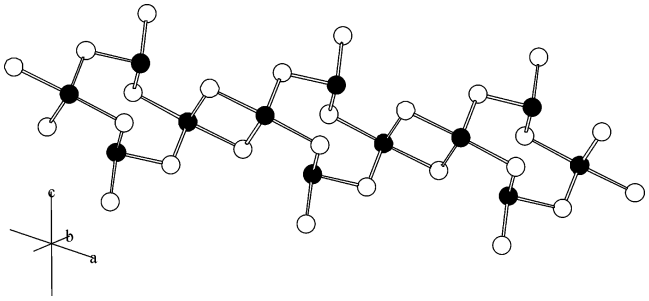

Figure 2. Single $Sb_4S_8^{4-}$ chain formed from the linkage of $Sb_4S_{10}^{8-}$ units through a common edge of the $Sb(2)S_4$ polyhedra: antimony, large black circles; sulfur, large open circles.

Sb(1)−S bond lengths in the range of 2.4100(7)−2.5390(6) Å. In addition, in common with the majority of other solvothermally prepared antimony sulfides, there is a further Sb−S interaction at the longer distance of 3.0697(7) Å, which is significantly less than the sum of the van der Waals' radii of Sb and S.[26] The coordination number of Sb(2) is however four, with two short (2.3839(7) and 2.4556(7) Å) and two longer (2.7119(8)−2.7520(7) Å) Sb−S bonds. Four-coordinate Sb(III) atoms, with a similar combination of two short and two somewhat longer Sb−S separations, have been previously observed in a number of solvothermally synthesized antimony sulfides.[27,28,29] Bond-valence sums for Sb(1) and Sb(2), calculated using the procedure of Brese and O'Keeffe,[30] are 2.95 and 3.07 v.u. respectively, consistent with the presence of Sb(III) in the framework.

Alternating vertex-linked $Sb(1)S_3^{3-}$ and $Sb(2)S_4^{5-}$ units generate $Sb_4S_{10}^{8-}$ clusters, containing Sb_4S_4 rings. Adjacent clusters are linked by sharing the two exocyclic sulfur atoms attached to Sb(2) to form $Sb_4S_8^{4-}$ chains (Figure 2). The S(4) atoms along the chain serve to link two sets of mutually perpendicular $Sb_4S_8^{4-}$ chains into a three-dimensional structure of stoichiometry $Sb_4S_7^{2-}$ (Figure 3). Along the crystallographic *c* axis, $Sb_4S_8^{4-}$ chains directed along [110] and [1-10] alternate and form a three-dimensional framework, which defines a network of three mutually perpendicular elliptical channels with approximate dimensions, measured from S(1) to S(1)′ and S(2) to S(2)′, of 2.4 × 9.2 Å, when the van der Waals' radius of S is taken into account.

Macrocyclic cations, doubly protonated to balance the charge of the antimony-sulfide framework, are located within these channels and are oriented with their molecular plane parallel to the channel direction. The location of hydrogen atoms in the difference Fourier maps revealed that the double protonation occurs at the two N(1) atoms of the macrocycle. N···S distances between the organic cation and sulfur atoms of the framework lie in the range 3.324(3)−3.884(3) Å. This is consistent with the presence of hydrogen bonding between the organic and inorganic components.

Reactions in the presence of transition-metal salts generate essentially the same antimony-sulfide frameworks in **2** and **3** as described above for **1**. Significant bond lengths and angles are presented in Table 3.

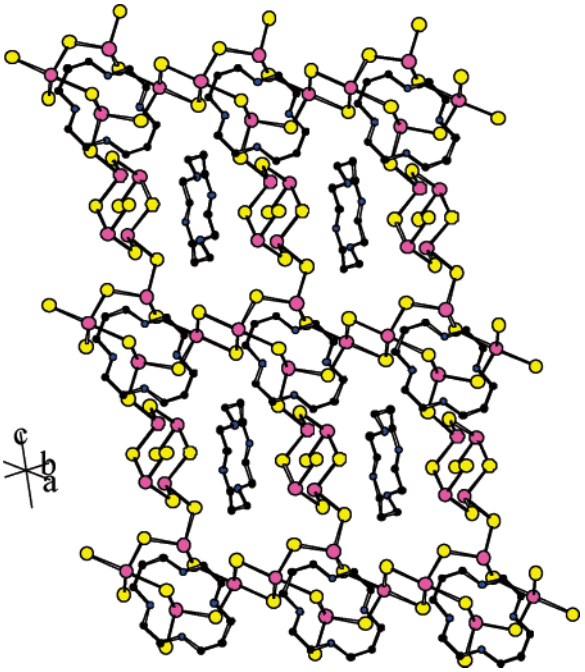

Figure 3. Linkage of $Sb_4S_8^{4-}$ chains directed along [110] and [1-10] through S(4) in **1** to form a three-dimensional $Sb_4S_7^{2-}$ network that defines a system of mutually perpendicular channels in which diprotonated macrocyclic cyclam cations reside: antimony, magenta; sulfur, yellow; carbon, black; nitrogen, blue.

Table 3. Selected Bond Lengths (Å), Angles (deg), and Bond Valences (v.u.) for $[Ni(C_{10}N_4H_{24})][Sb_4S_7]$ (**2**) and $[Co(C_{10}N_4H_{24})]_{1/3}[C_{10}N_4H_{26}]_{2/3}[Sb_4S_7]$ (**3**)[b]

	(2)		(3)	
		v^a		v^a
Sb(1)−S(1)^{i}	3.1091(17)	0.144	3.1018(12)	0.172
Sb(1)−S(1)	2.4127(16)	1.116	2.4116(12)	1.109
Sb(1)−S(4)	2.5155(15)	0.825	2.5269(11)	0.812
Sb(1)−S(2)	2.5002(17)	0.863	2.4920(12)	0.893
	Σ	**2.947**	Σ	**2.814**
Sb(2)−S(1)^{i}	2.7324(16)	0.436	2.7780(13)	0.412
Sb(2)−S(3)^{ii}	2.7350(17)	0.432	2.6914(13)	0.521
Sb(2)−S(2)	2.4487(18)	1.004	2.4514(12)	0.996
Sb(2)−S(3)	2.3802(18)	1.228	2.3888(13)	1.182
	Σ	**3.100**	Σ	**3.112**
S(1)^{i}−Sb(1)−S(1)	84.01 (5)		84.87(4)	
S(1)^{i}−Sb(1)−S(4)	171.68 (3)		173.51(3)	
S(1)−Sb(1)−S(4)	92.76 (5)		93.06(4)	
S(1)^{i}−Sb(1)−S(2)	82.69 (5)		83.75(4)	
S(1)−Sb(1)−S(2)	95.90 (6)		96.41(4)	
S(4)−Sb(1)−S(2)	90.04 (5)		90.38(4)	
S(1)^{i}−Sb(2)−S(3)^{ii}	176.11 (5)		175.28(4)	
S(1)^{i}−Sb(2)−S(2)	92.04 (5)		91.77(4)	
S(3)^{ii}−Sb(2)−S(2)	88.33 (6)		88.35(4)	
S(1)^{i}−Sb(2)−S(3)	89.46 (5)		88.43(4)	
S(3)^{ii}−Sb(2)−S(3)	86.68 (6)		86.93(4)	

[a] Bond valences and their sums calculated using parameters from ref 30. [b] Symmetry codes: (i) 2 − *x*, −*y*, −*z*; (ii) 3/2 − *x*, 1/2 − *y*, −*z*; (iii) 3/2 − *x*, −1/2 − *y*, −*z*; (iv) 2 − *x*, *y*, 1/2 − *z*.

In an analogous fashion to that of **1**, the macrocyclic cations in **2** and **3** are located in the channels created by the intersecting $Sb_4S_8^{4-}$ chains and are also oriented with their molecular planes approximately parallel to [1-10] (Figure 4). Both analytical electron microscopy and crystallographic

(26) Bondi, A. *J. Phys. Chem.* **1964**, *68*, 441.
(27) Engelke, L.; Näther, C.; Bensch, W. *Eur. J. Inorg. Chem.* **2002**, 2936.
(28) Volk, K.; Bickert, P.; Kolmer, R.; Schäfer, H. *Z. Naturforsch, Teil. B* **1979**, *34*, 380.
(29) Wang, X.; Liebau, F. *J. Solid State Chem.* **1994**, *111*, 385.
(30) Brese, N. E.; O'Keeffe, M. *Acta Crystallogr.* **1991**, *B47*, 192.

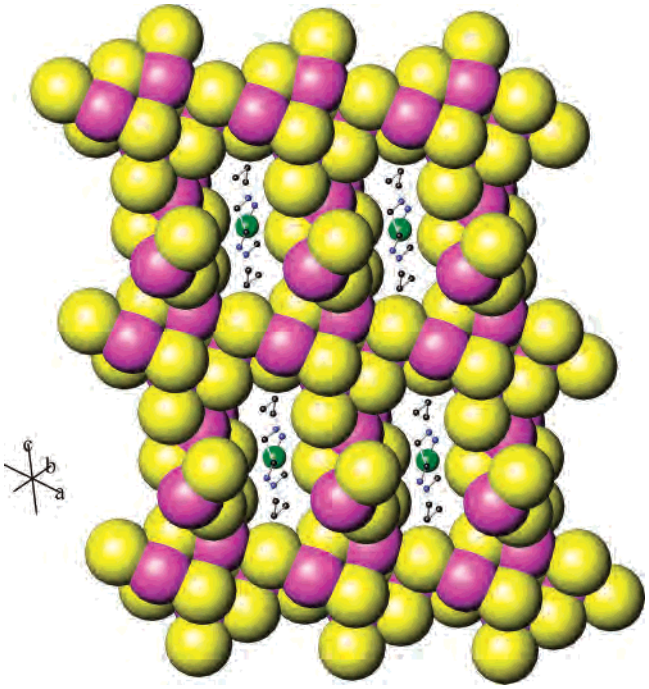

Figure 4. Space-filling representation of the $Sb_4S_7^{2-}$ framework of [Ni($C_{10}N_4H_{24}$)][Sb_4S_7] **(2)** illustrating one set of channels (parallel to [1-10]) and showing the location of the Ni^{2+}-chelate complex: antimony, magenta; sulfur, yellow; carbon, black; nitrogen, blue; nickel, green.

analysis are consistent with each macrocycle in **2** containing a Ni^{2+} ion, which therefore balances the charge of the framework, without the need for the macrocycle to be protonated. The nickel cations are coordinated by the four nitrogen atoms of the macrocycle with Ni−N distances of 1.947(6) and 1.952(6) Å, slightly shorter than those in discrete mononuclear complexes such as [Ni(cyclam)(O-COR)$_2$], (2.062(2)−2.074(2) Å).[31] The nearest sulfur neighbors are the two S(1) atoms of the framework above and below the plane of the complex at the rather long distance of 3.058(2) Å. This suggests that the Ni···S interaction is extremely weak (0.06 v.u.) and that the transition-metal complex is therefore essentially square planar. This conclusion is supported by room-temperature magnetic susceptibility measurements, which show the material to be diamagnetic ($\chi_{dia} \approx -4 \times 10^{-5}$ cm^3 mol^{-1}). The N···S distances (3.424(6)−3.848(6) Å) are comparable with those in **1**, implying similar hydrogen bonding interactions between the macrocyclic species and the antimony-sulfide framework.

The X-ray diffraction study of **3** produced a refined site-occupancy factor for the cobalt ion that signifies that the occupation of the site at the center of the macrocyclic ligand is incomplete. The average cobalt content, taken over crystallites in which the presence of cobalt was detected by analytical electron microscopy, is 0.4(2). Crystal structure analysis on five crystals selected from the same reaction product yielded cobalt site-occupancy factors in the range 0.213(4)−0.385(3), consistent with the presence of both metalated and nonmetalated forms of the macrocyclic species in the same crystal. The crystal for which details are reported here had a cobalt occupancy of 0.339(5). Again the transition-metal cation is four coordinate (Co−N = 2.010(5) and 2.0234(4) Å) with the nearest sulfur neighbors at 3.349(4) Å. The partial occupancy of this site (0.339(5)) leads to ambiguity in determining the oxidation state of the cobalt. At this level of cobalt incorporation, neither Co^{2+} nor Co^{3+} would be sufficient to balance the negative charge of the antimony−sulfide framework, and some degree of protonation of the uncomplexed amine present is necessary.

Attempts to distinguish between the two possible oxidation states using magnetic susceptibility measurements on hand-picked single crystals were rendered ineffective by the discovery of a magnetic-ordering transition at 113 K, which was assigned to CoS_2 (T_c = 110 K).[32] This trace ferromagnetic impurity, which is present as a fine coating on the crystals and therefore cannot be removed, dominates the magnetic response making it impossible to distinguish by magnetic measurements between square-planar Co^{2+}(S = 1/2) and Co^{3+} (S = 0). In situ oxidation in the hydrothermal reaction would be required to generate a Co(cyclam)$^{3+}$ complex from the $Co(O_2CCH_3)_2$ reactant. Indeed, examination of the literature indicates that in situ aerial oxidation is required for the preparation of mononuclear cyclam complexes of Co(III) from Co(II) reactants.[33] Given the reducing environment resulting from the production of H_2S as the reaction proceeds, oxidation therefore appears to be unlikely and hence we believe that the cobalt is present as Co^{2+}, the remaining positive charge being provided by protonation of the noncoordinated ligand.

To test this hypothesis further, [Co(cyclam)Cl_2]Cl, prepared by a literature route[33] involving aerial oxidation of an acidified methanolic solution of $CoCl_2 \cdot 6H_2O$, was used as a replacement (1.5 mmol) for $Co(O_2CCH_3)_2$ and cyclam in a solvothermal reaction analogous to that used for the preparation of **3**. The solid product of this reaction contained crystals of [Co($C_{10}N_4H_{24}$)]$_x$[$C_{10}N_4H_{26}$]$_{1-x}$[Sb_4S_7] (x = 0.014(3) and 0.011(3) from two single-crystal structure determinations), while analytical electron microscopy revealed a significantly lower cobalt content than that determined for **3:** the average Co:S ratio being only 0.02(2). UV−vis spectra (Figure 5) of the liquid phase of the reaction mixture, recorded on a Hel̀ios Spectronic Unicam spectrometer, were measured prior to and immediately following the reaction and compared with a spectrum obtained from an aqueous solution of Co(cyclam)Cl_2, also prepared using established procedures.[34] The Co(cyclam)$^{3+}$ complex in the initial reaction mixture is characterized by bands at 650 and 450 nm. After the reaction, these bands disappear completely. Although no peak is discernible in the post-reaction mother liquor, differential analysis of the spectrum identifies a feature at 538 nm, which compares favorably with the broad absorption at 533 nm in the spectrum of the Co(cyclam)$^{2+}$ complex in aqueous solution. We believe that the spectroscopic evidence

(31) Zakaria, C. M.; Ferguson, G.; Lough, A. J.; Glidewell, C. *Acta Crystallogr*. **2002**, *B58*, 78.
(32) Goodenough, J. B. *Magnetism and the Chemical Bond*; Wiley: New York, 1963.
(33) Bosnich, B.; Poon, C. K.; Tobe, M. L. *Inorg. Chem*. **1965**, *4*, 1102.
(34) Prakash, R.; Kandoi, S.; Srivastava, R. *Trans. Met. Chem*. **2002**, *27*, 598.

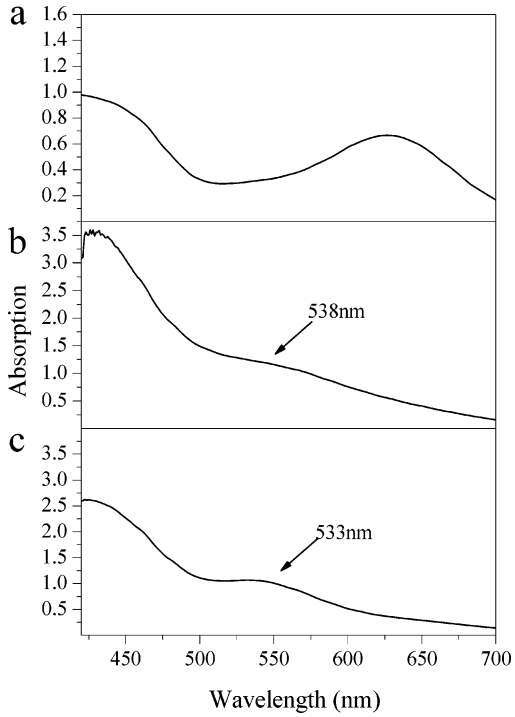

Figure 5. UV−vis spectra of $Co(cyclam)^{3+}$ (a) before and (b) after solvothermal reaction with Sb_2S_3 and S for 24 h and (c) the UV−vis spectrum of an aqueous solution of $Co(cyclam)Cl_2$.

demonstrates that the Co(III)-cyclam complex is not stable under the conditions of the reaction and therefore oxidation of Co^{2+} to Co^{3+} does not occur. Final evidence for the presence of Co(II) is provided by analytical electron microscopy data which reveal the presence of crystallites with Co:S ratios as high as 0.105. This corresponds to a site occupancy of 0.74, which for Co(III) would result in an excess of positive charge. Hence, **3** is formulated as Co(II)-containing $[Co(C_{10}N_4H_{24})]_x[C_{10}N_4H_{26}]_{1-x}[Sb_4S_7]$ ($0.08 \leq x \leq 0.74$) with the charge balance being achieved through double protonation of the noncomplexed macrocycle.

Measured stability constants for transition-metal cyclam complexes, $M(cyclam)^{2+}$ are very high ($\log K = 11.3$ to 27.2),[35] suggesting that differences in the stability of the transition-metal cyclam complexes do not play a significant role in determining the degree of metal incorporation in the phases reported here. This is further supported by our observations that introduction of $FeCl_2$ into the Sb_2S_3/S/cyclam reaction mixture produces single crystals of the same framework structure, with a lower metal content than for the cobalt-containing phase (among the 25% of examined crystals that contain iron, the maximum Fe:S ratio corresponds to an iron site occupancy of ca. 0.20), while the analogous reaction with $CuCl_2 \cdot 2H_2O$ leads to copper occupancies that vary over the wide range from 0.2 to 1.0, despite the stability constant for $Cu(cyclam)^{2+}$ being among the highest reported. Therefore, we believe that the lower level of cobalt incorporation in **3** compared to that of nickel in **2** is related to the ease of formation of the pyrite phase, CoS_2, which effectively removes cobalt from the reaction mixtures. No evidence for the formation of nickel-sulfide phases was observed in the powder X-ray patterns of the products containing **2**. However, the heterogeneous mixture that constitutes a solvothermal reaction inevitably entails a complex series of equilibria, as shown by the fact that using a salt of the transition-metal macrocycle complex as the source of transition metal and cyclam in the solvothermal reaction does not generally lead to products in which the degree of metal occupancy is complete. We are currently seeking to optimize reactions involving transition-metal ions other than cobalt and nickel in an effort to generate phases with higher levels of metal incorporation, a narrower spread of values, or both and will report on these in due course.

A striking feature of the three products reported here is the formation of a genuine three-dimensional structure, through the linkage of one-dimensional chains. Antimony sulfides typically exhibit a wide range of Sb−S distances (2.38−3.7 Å). Primary antimony−sulfur bonding distances are quite well defined: Sb−S distances in SbS_3^{3-} building units are typically <2.5 Å, while those in SbS_4^{5-} units containing two long and two short bonds, may extend to 2.8 Å. Longer secondary interactions in the range of 3.0−3.7 Å have also been invoked to link together higher structural units, although it should be noted that the contribution to the valence sum falls dramatically from 1.1 for an Sb−S bond of 2.4 Å to 0.4 at 2.8 Å and 0.1 at 3.2 Å. Thus consideration of only Sb−S distances < 2.8 Å leads to the identification of a wide range of chainlike structural motifs among solvothermally prepared antimony sulfides, especially those consisting of vertex-linked SbS_3^{3-} pyramidal units.[36] Structures of higher dimensionality generally only result from the interlocking of $Sb_xS_y^{z-}$ units by considering weaker (>2.8 Å) secondary Sb−S interactions.[7,19,29] The three-dimensional framework defined by antimony−sulfur bonds of <2.8 Å, as found in the materials reported here, is therefore highly unusual and represents only the second example, after $[Co(en)_3][Sb_{12}S_{19}]$,[13] of what we believe to be a truly three-dimensional system.

In summary, we have prepared the first members of a new series of macrocycle-templated antimony sulfides that adopt three-dimensional framework structures. This family represents a unique situation in antimony-sulfide chemistry, in which a structure-directing agent can generate both metalated and nonmetalated forms of the cationic species within identical anionic antimony-sulfide frameworks. The persistence of the framework into the metalated form suggests that this class of material may have applications as selective absorbents. In particular, the fact that access to the macrocycle in the noncomplexed form is restricted by the channel structure of the framework, may overcome the practical difficulties in using macrocyclic polyamines as selective metal-chelating agents because of the high stabilities of their complexes with most metal cations.

Acknowledgment. The authors thank the U.K. EPSRC for grants in support of a single-crystal CCD diffractometer

(35) Martell, A. E.; Hancock, R. D.; Motekaitis, R. J. *Coord. Chem. Rev.* **1994**, *133*, 39.

(36) Sheldrick, W. S. *J. Chem. Soc., Dalton Trans.* **2000**, 3041.

and a studentship for R.J.E.L. A.M.C. thanks The Leverhulme Trust for a Research Fellowship.

Supporting Information Available: Thermogravimetric data for **1** and **2**, and CIFs and listings of crystallographic data, atomic coordinates, bond distances and angles, and anisotropic thermal parameters for **1**, **2**, and **3**. This material is available free of charge via the Internet at http://pubs.acs.org.

IC060263F